PAPER • OPEN ACCESS

Synchrotron x-ray spectra characterisation for radiation therapy applications at the ESRF - ID17 biomedical beamline

To cite this article: Ilaria Di Manici *et al* 2024 *Phys. Scr.* **99** 065021

Physica Scripta

PAPER

Synchrotron x-ray spectra characterisation for radiation therapy applications at the ESRF - ID17 biomedical beamline

Ilaria Di Manici[1,2], **Juan Reyes-Herrera**[3], **Liam Day**[1,4], **Manuel Sánchez Del Río**[3], **Michael Krisch**[1] and **Paolo Pellicioli**[1,4]

[1] ID17 Biomedical beamline, European Synchrotron Radiation Facility, Grenoble, France
[2] Engineering Physics, Polytechnic University of Milan, Milan, Italy
[3] Advanced Analysis and Precision Unit, MEG-ISDD, European Synchrotron Radiation Facility, Grenoble, France
[4] Institute of Anatomy, University of Bern, Bern, Switzerland

E-mail: paolo.pellicioli@unibe.ch

Keywords: X-ray spectra characterization, synchrotron radiation, Monte Carlo simulation, dosimetry, half value layer method

OPEN ACCESS

RECEIVED
22 November 2023

REVISED
8 April 2024

ACCEPTED FOR PUBLICATION
26 April 2024

PUBLISHED
10 May 2024

Abstract

Objective. Radiation therapy requires reliable dosimetry protocols to deliver successful treatments with high accuracy and precision. In this context, accurate knowledge of the beam's energy spectra is mandatory. The goal of this study was to validate the synchrotron x-ray spectrum of the ID17 beamline at the European Synchrotron Radiation Facility (ESRF). The modification of the synchrotron storage ring and beamline in recent years necessitates a new characterisation of the radiation spectra of the ID17 beamline. The validated spectra will be a starting point for possible future clinical applications. *Approach*. The half value layer method was used to measure the attenuation of the x-ray spectrum in Al and Cu. Experimental data was validated against theoretical data produced using OASYS; an in-house developed software for calculating beamline spectra. Two different spectral configurations, 'conventional' and 'clinical', were investigated. The characterised spectra were used to perform dosimetric validation of depth dose profiles measured in a water-equivalent phantom. The dose profile was measured using two different detectors and compared with calculations generated using two different Monte Carlo algorithms. *Main results*. The results showed good agreement between measured and predicted half value layers, with differences of less than 1% in most cases. Excellent dosimetric agreement to within 3% was obtained, an agreement that satisfies the requirements in conventional radiotherapy for approvable treatment planning. *Significance*. Accurate spectra have been defined and validated for the ESRF—ID17 Biomedical beamline. The validated spectra can be used as input for future dosimetric studies and treatment planning systems in the context of preclinical studies and possible future clinical trials.

1. Introduction

Innovative radiation therapy (RT) approaches are currently being investigated using synchrotron radiation to take advantage of the incredible properties of this unique x-ray light. In synchrotron facilities, the high-intensity beam can deliver doses at ultra-high dose rates of up to tens of kGy s^{-1} and improve treatment outcomes compared to conventional radiotherapy using compact sources [1].

FLASH-RT is based on the administration of treatment doses in less than half a second [2]. This technique makes it possible to stop tumour growth and reduce the frequency and severity of early and late complications [3–6]. At present, synchrotron facilities are the most intense x-radiation sources capable of delivering the dose rates required to successfully exploit the FLASH effect.

Spatially fractionated radiation therapy (SFRT) modulates the field's intensity in the millimetre and submillimetre range, delivering highly heterogeneous dose distributions (in stark contrast to the homogeneous dose distributions delivered in conventional RT). The most extreme configuration of SFRT is called microbeam radiation therapy (MRT), in which the radiation beams are only a few tens of micrometres wide. MRT exploits

the dose-volume effect [7, 8], a phenomenon in which mature biological tissues tolerate high microbeam doses in the order of hundreds of Gy better than broad beam doses of only a few Gy. MRT has shown remarkable results in numerous preclinical studies compared to conventional radiotherapy, thanks to increased tolerance of healthy tissues and increased effectiveness in limiting tumour development [8–21].

MRT is currently performed at synchrotron sources, where the extreme radiation properties required to successfully deliver the microbeam doses are met: x-ray energy in the range of 100–200 keV to maintain the steep dose gradients, minimal beam divergence to keep the width of the beams in the microscopic range as they traverse the entire target, and ultra-high dose rates which reduce exposure times and mitigate the effects of organ motion on the dose distribution [22, 23].

The European Synchrotron Radiation Facility (ESRF) - ID17 Biomedical beamline, France [24] and the Australian Synchrotron - Imaging and Medical beamline (IMBL), Australia [25, 26] are the best equipped laboratories to perform MRT. MRT studies have also been successfully conducted at the Canadian Light Source - BioMedical Imaging and Therapy (BMIT) facility, Canada [27, 28] and at the Spring8 Japan Synchrotron Radiation Research Institute (JASRI) - BL28B2 beamline, Japan [29]. The PETRA III/DESY—P61A beamline, Germany, has recently developed a dedicated setup for MRT studies [30].

Robust and reliable dosimetry protocols are the foundation of any radiotherapy treatment, as high accuracy and precision on the dose delivered is essential for a successful outcome. Accurate knowledge of the x-ray energy spectrum used is a fundamental requirement, as the radiation dose delivered to the material also depends on the penetration depth of the incident photons and the mean free path length of the scattered electrons.

In this paper, the spectra characterisation of the ESRF - ID17 Biomedical beamline is presented together with a dosimetric validation under reference conditions. X-ray spectrum characterisation of the ID17 beamline has been investigated previously [31, 32], but renovation of the ESRF storage ring in 2019 (now EBS—Extremely Brilliant Source), combined with installation of new components on the ID17 beamline in preparation for veterinary trials, required a full characterisation of the x-ray spectra used for RT studies.

The starting point for the x-ray spectra calculation was the OASYS software developed at the ESRF for synchrotron beamline modelling and experiment simulation [33]. The characterisation of the spectra was then performed using the half value layer (HVL) method [34]. The newly defined spectra were used to validate the absolute dosimetry by examining the depth dose profiles delivered in a water-equivalent phantom with homogeneous broad beam fields. Verification of the agreement between simulated and measured doses was performed by comparing the data sets of two independent Monte Carlo simulations (MC) based on different dose calculation algorithms and two different experimental data sets using a PTW PinPoint ionisation chamber (IC) and radiochromic films. For completeness, the study was performed with two different spectra used for RT and MRT studies at the beamline.

This important study not only includes the use of the latest software for beamline modelling and methodology for absolute dosimetry at synchrotron sources, but also provides the entire work chain from spectra definition to validation of absolute dosimetry under reference conditions. Compared to previous dosimetry studies performed at the ID17 beamline, this work accounted fully for all PTW PinPoint IC correction factors. All data sets considered for HVLs and reference dosimetry agree within the typical 3% limit required by conventional RT [35]. Thus, this work is a fundamental step towards clinical applications at the ESRF - ID17 beamline for FLASH-RT and MRT studies.

2. Materials and methods

The characterisation of the ESRF - ID17 Biomedical Beamline spectra and the dosimetric validation of the defined spectra require the use of several techniques and a precise approach for both computational and experimental approaches. Before presenting all materials and methods in detail in the following sections, an overview of the workflow used is described. Section 2.1 describes the key components that characterise the beamline and are used to define the x-ray beam, while section 2.2 describes the software used to generate the beamline model and calculate the spectra profiles. The Half Value Layer (HVL) method is used to characterise the spectra and is described in section 2.3. To compare the calculated HVLs with the experimental ones, a PTW PinPoint Ionisation Chamber (IC) was used for the measurements and the protocol defined for the absolute dose measurements is described in section 2.4. A dosimetric validation of the defined spectra was performed by studying the depth dose profile (DDP) delivered by the photon beam to a water equivalent phantom. To validate the study, the results of two independent simulation approaches and two different detectors were compared. Monte Carlo (MC) simulations were used to estimate DDPs with the conventional radiation transport approach and with a so-called 'hybrid algorithm' specifically developed for MRT studies. Details of the simulation approaches are given in section 2.5. For the DDPs measurements, the PTW PinPoint IC mentioned above was used and section 2.6 describes the experimental setup used together with the reference conditions defined.

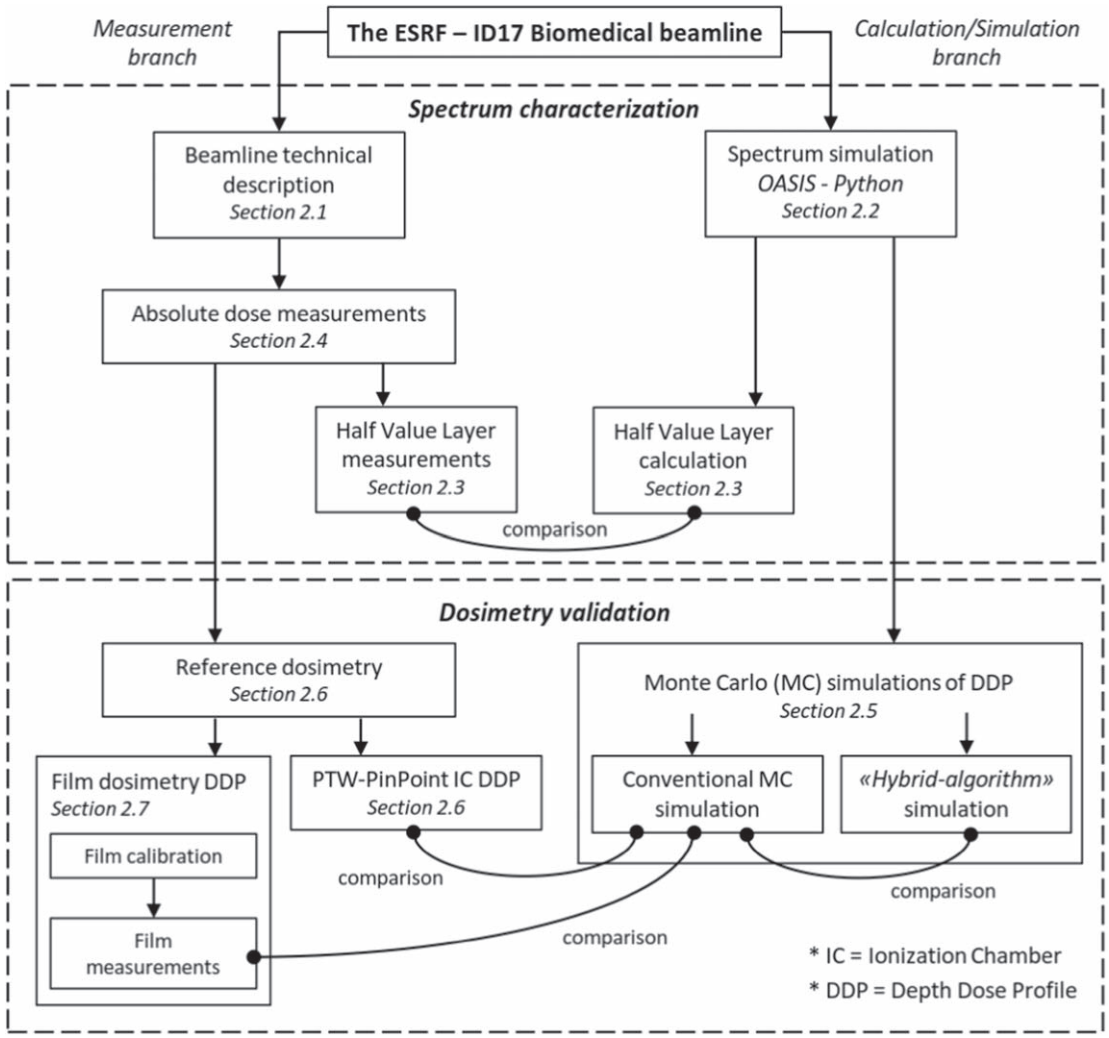

Figure 1. Flowchart of the procedure used for the characterisation of the ESRF - ID17 Biomedical beamline spectra and for the dosimetric validation of the defined spectra.

Radiochromic film dosimetry was used as a second detector for DDPs comparison, and its exposure procedure is described in section 2.7. Finally, the uncertainty budget is presented in section 2.8. The graphical representation of the workflow is presented in the form of a flowchart in figure 1.

2.1. The ESRF - ID17 biomedical beamline

The x-ray beam is generated by an electron current (up to 200 mA) in the synchrotron storage ring passing through the magnetic field of the 'w150' wiggler insertion device installed in the front-end section of the ID17 beamline. The wiggler source consists of two horizontal arrays, each with 10 magnets 15 cm long with alternating polarity. The vertical oscillating magnetic field strength can be up to 1.62 T with a gap of 24.8 mm between the two arrays; the typical wiggler gap used for RT studies on the beamline.

The synchrotron x-ray beam is transported in vacuum for approximately 37 m to the entrance of the experimental hutch, where the sample stage is located at a total distance of 40 m from the source. Low energy photons (below 50 keV) are filtered from the beam using five different attenuators made up of various thicknesses and materials, including C, Al and Cu. For beam monitoring during irradiation, two sets of ionisation chambers are utilised: a homemade pair of Compton scattering ICs [36] consisting of two pairs of Al plates each covered with a Au layer, called 'IC0', and a combination of two equivalent PTW Bragg peak chambers, called 'IC0bis'. To reduce wear-and-tear damage to the IC0bis detectors in preclinical radiotherapy experiments that do not require beam monitoring, PMMA can be used as a substitute to maintain the same beam quality. Dosimetry measurements were used to determine the thickness of PMMA that matches the attenuating effect of the IC0bis. The beam used for irradiation is defined by motorised slits and fixed apertures that collimate the synchrotron beam to select the more intense and homogeneous central part of the field. For this study, a 20 mm wide and 0.520 mm high radiation field-size was used. The final 20 mm high field at the

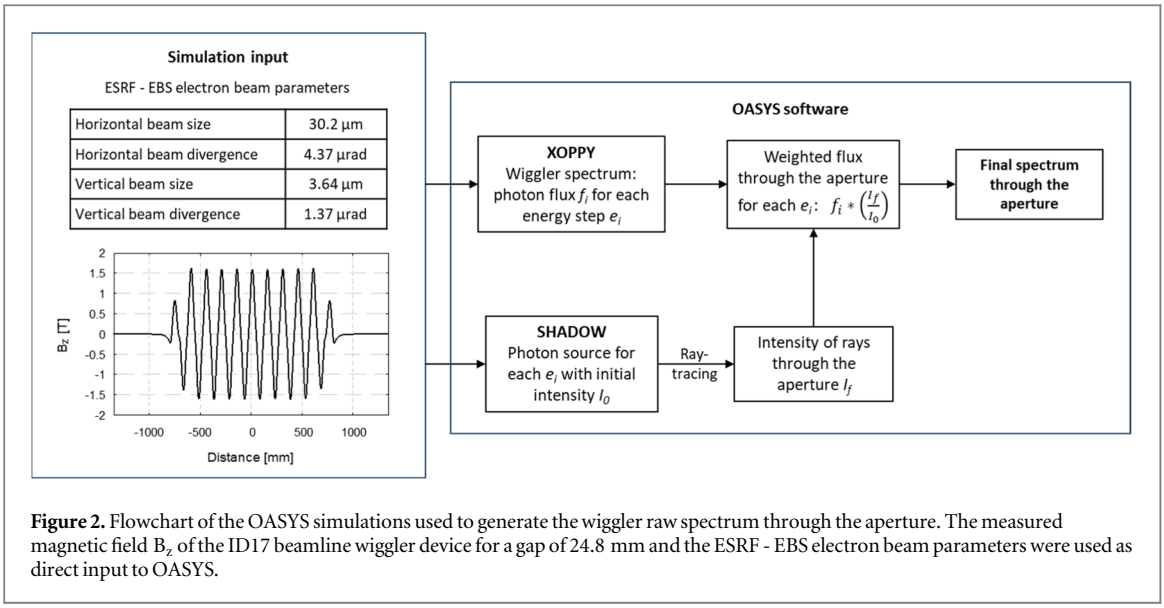

Figure 2. Flowchart of the OASYS simulations used to generate the wiggler raw spectrum through the aperture. The measured magnetic field B_z of the ID17 beamline wiggler device for a gap of 24.8 mm and the ESRF - EBS electron beam parameters were used as direct input to OASYS.

target is achieved by positioning the sample on a motorised stage and scanning it vertically through the beam during the irradiation.

Results are reported for the two main spectral configurations used for MRT studies on the beamline: the so-called 'conventional' spectrum used for pre-clinical MRT studies, and the 'clinical' spectrum used for experiments with clinical scenarios [37]. In the conventional setup, no monitoring devices are used, and the filter configuration is as follows: 1.13 mm carbon, 1.45 mm aluminium, and 0.98 mm copper. The second configuration is achieved by adding 0.9 mm filter copper to harden the x-ray spectrum and by placing the two monitoring devices (IC0 and IC0bis) into the beam path.

2.2. X-ray spectra simulation

The wiggler raw spectrum through the final aperture was calculated using OrAnge SYnchrotron Suite (OASYS) software, version 1.2 [33]. OASYS is a collection of tools and libraries designed for the analysis and simulation of synchrotron radiation sources and beamlines. This code is developed and maintained by the ESRF and the Advanced Photon Source (USA). OASYS is widely used in the field of synchrotron radiation research for tasks such as beamline design, x-ray optics simulations, and data analysis. For these simulations, two OASYS packages were used, a Python version of XOP [38]—XOPPY—and SHADOW.

The initial wiggler spectrum was calculated with XOPPY using the magnetic field of the wiggler and the electron beam parameters of the ESRF—EBS [39]. For the first time at the beamline, the wiggler magnetic field (B_z) used for the simulation was measured using a Gaussmeter placed at the center of the 24.8 mm wiggler gap. The wiggler spectrum was calculated over an energy range of 0.1 keV to 600 keV, since above 600 keV the raw spectrum shows an intensity five orders of magnitude smaller than the maximum intensity and can be considered negligible for our investigations. The energy range was sampled in N = 6000 energy steps e_i corresponding to an energy delta of 0.1 keV.

A ray source was generated in SHADOW using the wiggler B_z and the electron beam parameters. For each energy step e_i, an initial number of rays I_0 were ray traced through the aperture producing a final intensity I_f. The final spectrum at the aperture was obtained by weighting the initial wiggler spectrum by the ratio of initial and final intensities I_0/I_f for each e_i. Figure 2 shows the calculation scheme used by OASYS software.

The raw flux spectrum through the aperture obtained from OASYS served as input to an in-house developed Python code that calculates the attenuation of the x-ray beam through the beamline's attenuators and monitoring components. The Python code was developed using the XRayDb library, which provides data from the NIST database for material attenuation coefficients [40]. By modifying the filter parameters, all different spectrum configurations can be calculated.

2.3. Half value layer (HVL) method

The HVL (Half Value Layer) method, widely used in clinical radiotherapy, was used to validate the calculated polychromatic spectra [34]. The photon beam quality is defined by measuring the thickness of the absorber (filter) required to halve the initial beam intensity. This filter thickness is called HVL. For spectra in the orthovoltage range, Al and Cu filters are typically used for the measurement. The second and third HVL reduce the beam intensity to 25% and 12.5% of its original value. As the average energy of the beam increases as it passes

through the filters (the spectrum becomes *harder*), each HVL is smaller than the next. Although the HVL measurements do not provide the spectral profile, the spectral validation was performed by comparing the measured HVL data with the calculated theoretical data.

HVL measurements were obtained using layers of Cu or Al with a purity of 99.999% and a total thickness from 0.39 to 10.21 mm for Cu and from 1.97 to 52.60 mm for Al. The transmitted radiation through the additional metallic material was measured with a PTW 31014 PinPoint IC. To calculate the exact values of HVL1, HVL2, and HVL3, corresponding to 50%, 25%, and 12.5% transmittance of the original beam, respectively, the following quadratic curve was fitted to the experimental data:

$$y = a_2x^2 + a_1x + a_0 \tag{1}$$

where,

$$x = -\ln\left(\frac{I}{I_0}\right) \tag{2}$$

and I is the transmitted intensity. Here $a_0 = 0$, and $y = 0$ when $I = I_0$. Corresponding HVLs were calculated for comparison using the Python script described in section 2.2.

2.4. Absolute dose measurements

The PTW 31014 PinPoint IC has been well characterised and is routinely used at the ID17 beamline for absolute dosimetry under reference conditions with homogeneous fields [41]. Since the target is scanned through the beam to generate the full 20×20 mm^2 field, the dose is measured by integrating the PinPoint signal over the entire irradiation while the chamber is scanned in tandem with the phantom. An $N_{d,w}$ conversion factor (based on the calibrations provided by PTW for 'TH' series of beam qualities) is used to convert the PinPoint signal to dose to water. The dose rate may then be calculated from the measured PinPoint dose as:

$$\dot{D} = \frac{D \times v}{z_{beam}} \tag{3}$$

where z_{beam} is the beam height and v is the vertical scan speed, which was fixed at 20 mm s^{-1} for the measurements. Three measurements were taken for each additional layer of material added into the beam path. The measured dose was normalised by the storage ring current at the time of irradiation, obtaining the normalised dose D_n[Gy mA^{-1}]. The intensity ratio (IR) for each additional layer of material was calculated by dividing the normalised dose D_n, by the value of the normalised dose D_{n0} measured with no additional material layers present. The IR curve for each spectrum was obtained by increasing the thickness of the additional layers in the beam path.

Measurements made with the PinPoint IC include correction factors for temperature and pressure variations, variations in mean beam energy, polarity effect, ion recombination, and electrometer calibration as defined by the IAEA TRS 398 protocol [42]. The correction factor accounting for the ion recombination $k_s$was re-measured for the PTW PinPoint IC used. The k_s factor is critical for ionization chamber measurements at high dose rates as it accounts for the incomplete collection of charges during the detector measurement. The higher the dose rate, the larger the ks factor that must be applied to the measured value. The ramping approach established by Fournier *et al* [41] was followed for ion recombination measurements. This approach was developed to account for the unique characteristics of the synchrotron photon flux and is based on measurements with increasing storage ring current and consequently increasing dose rates, while keeping the spectral profile constant. Synchrotron currents in the range 10–200 mA, with steps of 10 mA, was used for the measurements.

For this study, the application of some correction factors was revised and improved upon compared to previous work by Fournier *et al* [41]. Temperature and pressure variations affect the mass of air contained in the ionization chamber and therefore the amount of current generated by a given amount of radiation delivered to the detector. A correction factor $k_{T,P}$ is defined to account for measurements in atmospheric conditions different from those defined during the detector calibration. The IAEA TRS 398 protocol [42] defines $k_{T,P}$ as follows:

$$k_{T,P} = \frac{(273.2 + T)}{(273.2 + T_0)}\frac{P_0}{P} \tag{4}$$

Where T_0 and P_0 are the temperature and pressure measured during the detector calibration procedure and T and P are referring to the atmospheric conditions at the time of the measurement. Temperature and pressure were recorded at each detector reading and $k_{T,P}$ was calculated for each measurement, rather than considering only the initial temperature and pressure to define a unique $k_{T,P}$ to be applied to all measurements. This approach resulted in less error-prone measurements. A total temperature variation of 2.4 °C was observed during the experiment, which, if not properly considered, represents a potential 0.8% error in the measured dose. This uncertainty value is higher than the 0.3% suggested by Fournier *et al* [41].

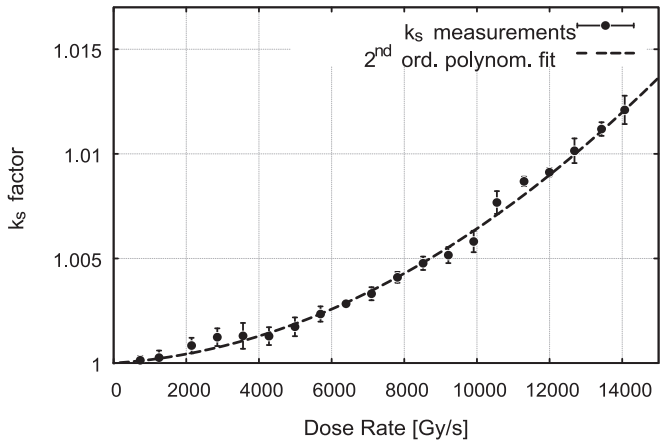

Figure 3. k_s values as function of the dose rate for the PTW PinPoint IC. k_s values are obtained by the current ramping approach [41] and include an accurate correction for temperature and pressure variation for each measurement point.

Five measurements were acquired for each dose rate data point, and the 2σ standard deviation for each data point was no more than 0.07%. The new k_s values obtained as a function of dose rate are shown in figure 3. Considering the 20 experimental points N_d, a quadratic curve fits the experimental data with a χ^2/N_d value of 2.5, where almost half of the χ^2/N_d value is due to the contribution of the point at 11.3 kGy/s.

For the first time at the ID17 beamline, an energy correction considering the calculated polychromatic spectrum profile, in combination with the energy correction factors of the PTW 'TH' beam quality series, was used for reference dosimetry measurements. Practically, a weighted average between the correction factor k_Q of the PTW 'TH' beam quality series and the corresponding photon intensity, was used to define the final calibration factor for the absorbed dose to water of the detector [43]. The k_Q factor may differ by up to 1.4% if only the 'TH 200' beam quality calibration factor is considered to characterize the whole polychromatic spectrum, as it was done in the work of Fournier *et al* [41].

2.5. Monte Carlo simulations of depth dose profile

Dosimetry validation was performed using the depth dose profile (DDP) method, comparing simulated and measured doses delivered at different depths within a target volume.

Monte Carlo (MC) simulations were performed with two different and independent approaches: the conventional MC algorithm which explicitly transports both photons and electrons individually, and the so-called 'hybrid' algorithm, a newer approach developed by Donzelli *et al* [44], which transports photons via MC, but uses an analytically calculated electron kernel to compute the final dose deposited. The hybrid algorithm decreases the dose calculation time significantly without losing accuracy.

The conventional MC simulation was performed on the ESRF computational cluster using the Geant4 toolkit version 10.03.p03 selecting the physics model PENELOPE [45, 46]. The threshold for secondary production was set at 1 μm for both MC approaches. For the calculation, the $180 \times 180 \times 180$ mm^3 volume of water used for the DDP measurements was constructed as simulation geometry, containing an internal scoring volume with dimensions $180 \times 30 \times 30$ mm^3, and resolution $1 \times 1 \times 1$ mm^3. For both spectra, doses were calculated by simulating 20×10^9 photons. The dose profile was obtained by averaging the dose at different depths in the centre of the irradiation field over a volume of 16 mm^3, which is similar to the 15 mm^3 active volume of the PTW PinPoint IC used.

The hybrid dose calculation algorithm was previously paired with the Eclipse^{TM} treatment planning system (Varian Medical Systems, inc.), a commercially available graphical software routinely used for treatment planning in the clinic [47, 48]. Eclipse^{TM} was used to generate the phantom geometry and display the dose distribution, while the dose calculation was performed using the hybrid algorithm engine. The calculation resolution for the Eclipse-hybrid algorithm was kept the same as for the conventional MC simulations, (i.e. 1 mm^3), but only 2×10^9 photons were simulated to keep computation times below 2 h.

Since the synchrotron radiation source is a few tens of microns in size and 40 m away from the target, the parallel beam approximation was used to define the irradiation beam in the conventional MC approach. In addition, the intensity profile of the beam was modelled as homogenous, since the beam intensity drops by only 0.5% at 5 mm from the beam axis and by 2.1% at 10 mm. This approximation was used for several years to model the ID17 beam. Instead, a more realistic beam geometry was generated using the Eclipse^{TM} software. Based on the dimensions of the electron beam of the storage ring, a radiation source with a Gaussian profile was

defined. The divergence of the photon beam is of 0.500 mrad horizontally and 0.013 mrad vertically, and this was implemented in the model of the beam geometry.

2.6. Reference dosimetry

DDPs were measured using absolute dosimetry with a PTW PinPoint IC and the LAP EASY CUBE phantom, a cubic phantom of $180 \times 180 \times 180$ mm^3 volume composed of 1 cm thick water-equivalent plastic plates. One of the plates was designed with a dedicated cavity to accommodate and accurately fit the PTW PinPoint IC. The cube was placed on the goniometer stage and aligned so that the PinPoint IC was centred in the beam path. During irradiation the phantom and PinPoint IC were scanned vertically over the full 20×20 mm^2 field size. Three measurements were taken at depths of 10, 20, 40, 60, 80, 100, 120, 140, 160, and 170 mm inside the cube. The *IR* curve of the measured dose values was normalised with the measured value under reference conditions (i.e., at 2 cm depth).

2.7. Film dosimetry

A second set of measurements was acquired using radiochromic film dosimetry. Radiochromic films are well-known detectors and gold-standard dosimeters in conventional RT, and their ability to resolve micron-scale dose variations makes them suitable detectors for MRT dosimetry [49]. GAFchromic^{TM} HD-V2 films were used for this study. The films were irradiated after being placed inside the EASY CUBE phantom and taped to the surface of the plates, at the same depths chosen for the absolute dosimetry. Three separate films were exposed at each position.

After irradiation, the films were digitised with a flat panel scanner and analysed with in-house developed MatLab codes that mapped the optical density to a dose value, following a previously established protocol [50]. To convert the optical density to dose, a calibration curve was created by irradiating a series of films under reference conditions in the range of 0–400 Gy, fully encompassing the doses delivered in the DDP measurements.

2.8. Uncertainty budget

The OASYS-Python calculated spectra had an uncertainty of 2% (2σ) in the mass attenuation coefficients obtained from the NIST database [51]. The thickness of the beamline filters was measured to an accuracy of $\pm$ 1 μm and the standard deviation over five measurements is approximately 0.3%. Taking into account a 2% (2σ) variation in all attenuation coefficients and a 0.6% (2σ) variation in the thickness of each of the filters used to define the spectra, the calculated variation in the mean energy of the spectrum is approximately $\pm$ 0.6%. When performing the DDP calculation with conventional MC simulations (data not shown), the maximum difference in the delivered dose between the spectrum obtained with theoretical attenuation and the shifted mean energy spectrum is about $\pm$ 0.5% at the phantom entrance and increases to about 1.1% at the phantom exit.

For HVL theoretical values, an overall uncertainty of 2.55% (2σ) was calculated accounting for the mass attenuation coefficients and thickness of the beamline attenuators uncertainty. For HVL measurements, an overall uncertainty of 4.76% (2σ) was applied to the thicknesses of the components along the beam path, including beamline attenuators and monitoring devices, and additional aluminium or copper layers. This error budget includes the uncertainty of the calliper measurement for the thickness of 0.5%; an error in vertical slit size of 0.19%; and an uncertainty in component position of 0.8% [32]. For the PinPoint IC dosimetry, the error in all correction factors was provided by Fournier *et al* [41], except for the k_s factor, which was recalculated and fixed at 0.07%. The total uncertainty at 2σ for the PinPoint IC measurements is thus 3.88% for the HVL measurements. The larger contribution to the PinPoint IC uncertainty is related to the dose-to-water calibration factor provided by PTW that is equal to 3.7% (2σ). The overall uncertainty for HVL measurements is thus 6.14% (2σ).

For the DDP measurements, the uncertainty on the PinPoint IC acquisition is of 4.16% (2σ), accounting also for the uncertainty associated with positioning of IC inside the phantom. For radiochromic films, the uncertainty is 5.02% (2σ), accounting for the uniformity guaranteed by the vendor and the uncertainty due to the scanning process after irradiation. For Monte Carlo simulations, the worst-case uncertainty at 2σ is 0.66% for the conventional algorithm and 1.06% for the hybrid algorithm.

3. Results

3.1. Simulated spectra

Figure 4 shows the raw spectrum calculated using OASYS after passing through the 20×0.52 mm^2 slits, together with the subsequent Python-calculated conventional and clinical spectra. The spectra are expressed as flux [Photons s^{-1} 0.1%BW^{-1}] normalised by the maximum ESRF storage ring current (200 mA) and the area of the

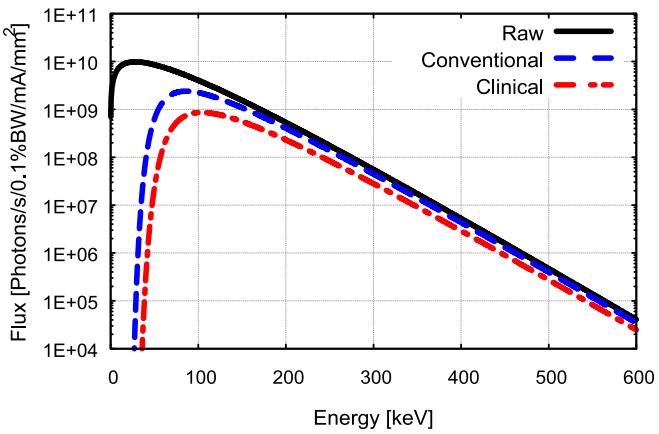

Figure 4. X-ray spectra profiles from OASYS (raw) and after the attenuating elements simulated with the Python code (conventional and clinical).

Table 1. The average energy, peak energy, and measured dose rate for the conventional and clinical spectra.

Spectrum	Average energy [keV]	Peak energy [keV]	Dose rate [Gy s^{-1}]
Conventional	101.8 ± 0.6	85.8 ± 0.5	$15\,699 \pm 9$
Clinical	120.0 ± 0.7	102.2 ± 0.6	$6\,045 \pm 4$

slits, i.e., [Photons s^{-1} 0.1%BW^{-1} mm^{-2} mA^{-1}]. Moving from the raw spectrum to the conventional spectrum, all photons below an energy of approximately 50 keV are clearly cut off by the filter components. The rapid decrease in the intensity of the spectrum at higher energies is a peculiarity of the synchrotron wiggler source. The clinical spectrum is harder than the conventional spectrum due to the additional Cu filter thickness and monitoring devices in the beam path. Table 1 shows the average energy, peak energy, and dose rate measured by the PTW PinPoint IC in air for the two spectra used for radiotherapy studies. The measured dose rates are reported with the standard deviation uncertainty calculated over five measurements. The study of the transversal variation of the spectrum energy was as well possible with OASYS software by computing the spectrum over a selected small portion of the aperture, more specifically 1 mm wide and 0.520 mm high. At 5 mm from the central axis, the spectrum mean energy is about 0.1% less than the value at the central position, and at 10 mm from the central axis, it is 0.4% less. The expected spectrum mean energy variation at the lateral end of the used aperture is smaller than the one expected from the uncertainty defining the spectrum profile and reported in section 2.8.

3.2. Half value layer (HVL)

Figure 5 shows *IR* profiles through Cu and Al, for both the conventional and clinical configurations. The bottom graph shows the percent deviation of the experimental data from the theoretical data. The average difference between experimental and theoretical data is less than 1.2% for each data set, with each point individually remaining below 2% for both Al and Cu HVL measurements.

Table 2 shows the HVL1, HVL2, and HVL3 extrapolated from an exponential fit to the experimental data and compared to their respective theoretical values for all combinations of spectral configuration and material. The percentage deviation between fitted experimental HVLs and theoretical HVLs again remains below 2%, and is below 0.8% on average, for each spectrum configuration.

The HVL method was also used to confirm the equivalence in attenuation of the beam between IC0bis and 22 mm of PMMA (data not shown). HVLs were measured in the clinical configuration using either the monitoring device (IC0), the two PTW Bragg peak chambers (IC0bis), or the 22 mm of PMMA. The two resulting IR curves are in close agreement having 1% difference at maximum, and below 0.5% for most data points, confirming the hypothesis of equivalence.

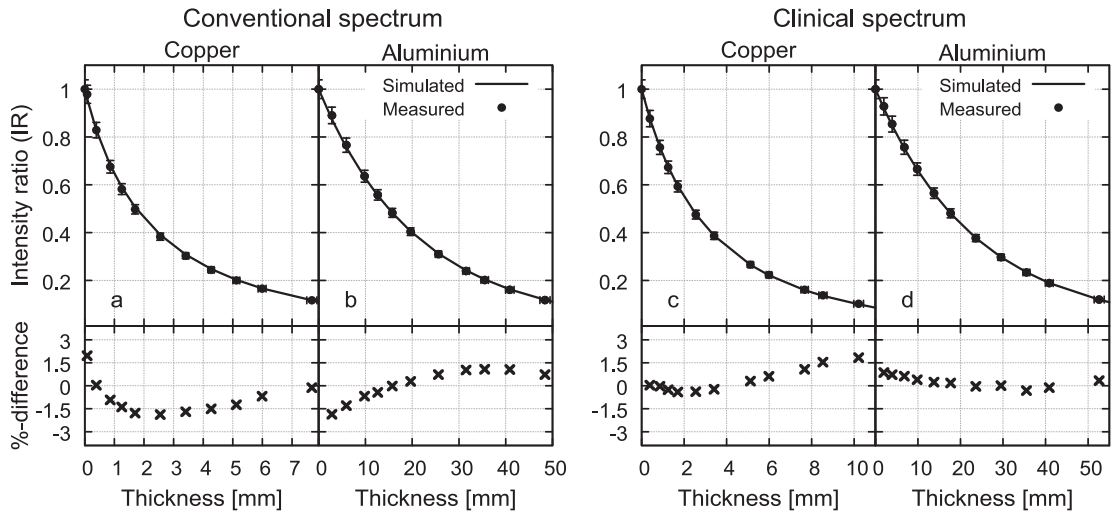

Figure 5. Comparison between calculated and measured intensity ratio curves obtained for Cu and Al for (a), (b) conventional spectrum and (c), (d) clinical spectrum. Below each intensity ratio curve, the percentage deviation of the measured data from the theoretical data is shown.

Table 2. HVL1, HVL2, and HVL3 of Cu and Al obtained by fitting experimental data are compared with theoretical predictions for the conventional and clinical spectrum.

Conventional spectrum						
	Copper			Aluminium		
	Experimental [mm]	Theoretical [mm]	%-diff.	Experimental [mm]	Theoretical [mm]	%-diff.
HVL1	1.71 ± 0.10	1.74 ± 0.04	−1.72	14.99 ± 0.92	14.97 ± 0.38	0.13
HVL2	4.16 ± 0.26	4.24 ± 0.11	−1.89	30.64 ± 1.88	30.76 ± 0.78	−0.39
HVL3	7.36 ± 0.45	7.36 ± 0.19	0.00	46.94 ± 2.88	47.24 ± 1.20	−0.64
Clinical spectrum						
	Copper			Aluminium		
	Experimental [mm]	Theoretical [mm]	%-diff.	Experimental [mm]	Theoretical [mm]	%-diff.
HVL1	2.37 ± 0.15	2.37 ± 0.06	0.00	16.73 ± 1.03	16.69 ± 0.43	0.24
HVL2	5.40 ± 0.33	5.40 ± 0.14	0.00	33.91 ± 2.08	33.88 ± 0.86	0.09
HVL3	9.08 ± 0.56	8.99 ± 0.23	1.00	51.54 ± 3.16	51.54 ± 1.31	0.00

3.3. Monte Carlo simulations

Figure 6 shows the DDP comparison between the two independent Monte Carlo algorithms and the dose measurements used for the two spectral configurations. The differences between the two MC simulated dose profiles remained below 1% for most points and increased only slightly to approximately 2% near the phantom exit. The dose profiles are normalised to the reference depth at 2 cm for comparison. The uncertainties for both simulations are very small, as described in section 2.8, and so error bars are not included for the MC data.

3.4. Dosimetry validation

The DDP simulation using the conventional MC algorithm serves as a reference for comparison with the dosimetry measurements using the PinPoint IC and the radiochromic films. The results are shown in figure 6 for both the conventional and clinical spectra. The PinPoint IC dosimetry measurements deviate from the MC data by less than 0.96% on average for each data set, and by less than 2% for each individual acquisition. For film dosimetry, the results show a difference between measurement and MC simulation data of less than 2.25% on average for each data set, with most data points differing by less than 3%. Only a few outliers deviate from simulation by approximately 4%. Each measured data point is in excellent agreement with the MC simulation and is well within the measurement uncertainties.

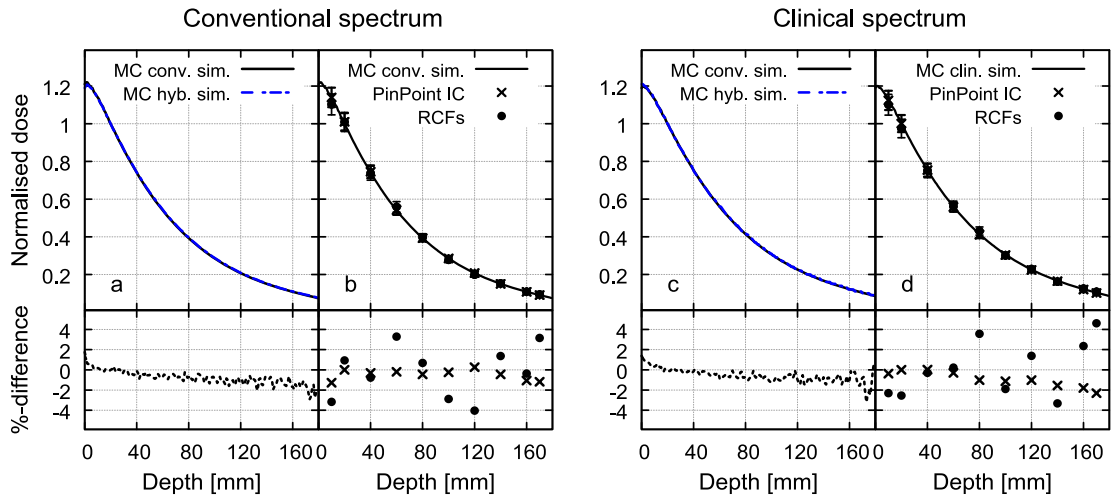

Figure 6. DDP comparison between the two different Monte Carlo simulations (conventional and hybrid algorithms, black and blue lines respectively) and two dose measurements with PinPoint IC (crosses) and radiochromic films (RCFs). Dose profiles are normalised to 1 at 20 mm depth. The percent difference between the data sets is given below each DDP. The simulation using the conventional approach MC (black line) was considered as the reference data set. The results are given for the (a), (b) conventional and (c), (d) clinical spectra used.

4. Discussion

We have characterised the energy spectrum profile of the ESRF—ID17 Biomedical Beamline, where innovative radiotherapy research is performed. The HVL method was applied and resulted in excellent agreement to theoretical data, with a worst-case deviation of approximately 2% and less than 1% for most data points. The calculations were performed using the OASYS software, which has proven to be an effective and reliable tool for spectral simulation. However, the Shadow library, used for the ray tracing simulation, requires a large number of rays to obtain precise and accurate results. The study of an analytical approach that can reduce the computation time while maintaining the same reliability and level of detail is already underway. With this new approach, it would also be possible to perform the complete simulation of the beamline directly on the OASYS platform, without needing to resort to additional Python code layers to account for the extra attenuation.

To our knowledge, the full use of all correction factors for the PinPoint IC measurements has not been done previously for synchrotron radiation dosimetry and showed a significant improvement in the quality of the results. Overall, it can be stated that the results are an improvement of the work previously performed by Crosbie *et al* [32] and is a successful validation of the OASYS software for future studies.

The HVL measurements confirm the equivalence between the two Bragg peak chambers and 22 mm of PMMA in terms of radiation attenuation. Thus, the PMMA can be used instead of the detectors when the monitoring functions are not needed to prevent their degradation.

Ten years after the work of Crosbie *et al* the beamline modification has affected the beam quality. The mean energy and peak energy of the clinical spectral configuration increased by approximately 10 keV and this is clearly reflected in the HVL values, which are up to 19% higher in this study. Considering the work of Pellicioli *et al* [52] on radiation transmission through the multislit collimator blades when MRT is performed on the beamline, it was also important to extend the spectrum calculation at energies above 400 keV, the upper limit defined by Crosbie *et al* in their work, to properly define all the radiation contributions that determine the final delivered dose.

The DDP validation provides confidence in the dose delivery for homogeneous synchrotron radiation fields in water-equivalent phantoms and shows accurate modelling of the synchrotron spectra. The two MC simulation algorithms showed good agreement, with differences of no more than 1%. This confirms that the hybrid algorithm can be used in place of the conventional MC approaches to speed up the computation time while maintaining high reliability. The remaining difference between the two approaches can be explained by the different physics libraries used during code development and the different beam geometry models implemented.

The DDP measurements obtained using the PTW PinPoint IC detector show excellent agreement compared to the MC simulation data. The use of all correction factors for the IC readout significantly improved the agreement between the data sets and should always be considered. Dosimetry with radiochromic films also provided convincing agreement, with deviations from expected values of less than 3% for most data points.

Accurate measurement with radiochromic films is critical since it is relied on to perform routine dosimetry of broad beam fields and is the primary radiation dosimeter for measuring microscale dose distributions. Dose readings from irradiated films require multiple passes of analysis post-irradiation, which introduces several possible sources of error. Although film measurements were repeated several times and averaged to reduce statistical variation, there are still higher variations in film readings than from the PinPoint IC data. A more rigorous protocol could be implemented to reduce the uncertainties in the readout of the film related to possible inhomogeneities of the active material.

5. Conclusions

Clinical trials in synchrotron RT requires highly robust and reliable dosimetric protocols, and therefore a precise knowledge of the spectrum is a fundamental necessity. This study characterized the x-ray spectra at the ESRF - ID17 Biomedical beamline for future RT studies following the recent renovation of the synchrotron storage ring and beamline.

The HVL method was used to successfully validate the spectra by comparing experimental results with spectra calculated using the OASYS software. The close agreement between experimental and calculated HVL values to within 2% proves the reliability of the OASYS software in simulating the ID17 beamline spectrum. The complete use of correction factors for the IC measurements strengthened the agreement with MC simulation data and improved the results compared to previous work on the beamline [32].

With the newly defined spectra, dosimetric validation was performed by measuring depth dose profiles for synchrotron broad beam radiation fields in a water-equivalent phantom. The experimental results were compared to MC simulations. The overall agreement between all four data sets was excellent and within the 3% level typically required for clinical radiotherapy dosimetry [35]. The few outliers observed with the radiochromic film dosimetry were expected due to the complexity and uncertainties associated with the protocol.

The newly defined spectra provide a reliable basis for synchrotron RT dose calculation and treatment planning, and facilitates potential clinical trials for MRT at the ESRF - ID17 Biomedical beamline.

Data availability statement

All data that support the findings of this study are included within the article (and any supplementary files).

ORCID iDs

Paolo Pellicioli https://orcid.org/0000-0003-3590-116X

References

[1] Blattmann H *et al* 2005 Applications of synchrotron x-rays to radiotherapy *Nucl. Instrum. Methods Phys. Res.* A **548** 17–22
[2] Durante M, Bräuer-Krisch E and Hill M 2018 Faster and safer? FLASH ultra-high dose rate in radiotherapy *Br. J. Radiol.* **91** 20170628
[3] Miles D *et al* 2023 FLASH Effects induced by orthovoltage x-rays *Int. J. Radiat. Oncol. Biol. Phys.* **117** 1018
[4] Favaudon V *et al* 2014 Ultrahigh dose-rate FLASH irradiation increases the differential response between normal and tumor tissue in mice *Sci. Transl. Med.* **6** 1–10
[5] Bourhis J *et al* 2019 Treatment of a first patient with FLASH-radiotherapy *Radiother. Oncol.* **139** 18–22
[6] Montay-Gruel P *et al* 2018 X-rays can trigger the FLASH effect: ultra-high dose-rate synchrotron light source prevents normal brain injury after whole brain irradiation in mice *Radiother. Oncol.* **129** 582–8
[7] Zeman W, Curtis H J and Baker C P 1961 Histopathologic effect of high-energy-particle microbeams on the visual cortex of the mouse brain *Radiat. Res.* **15** 496
[8] Laissue J A *et al* 2001 The weanling piglet cerebellum: a surrogate for tolerance to MRT (microbeam radiation therapy) in pediatric neuro-oncology *Penetrating Radiation Systems and Applications III.* ed H B Barber *et al* **4508** 65–73
[9] Adam J-F *et al* 2022 Toward neuro-oncologic clinical trials of high-dose-rate synchrotron microbeam radiation therapy: first treatment of a spontaneous canine brain tumor *Int. J. Radiat. Oncol. Biol. Phys.* **113** 967–73
[10] Eling L *et al* 2021 Unexpected benefits of multiport synchrotron microbeam radiation therapy for brain tumors *Cancers (Basel).* **13** 1–16
[11] Eling L *et al* 2019 Ultra high dose rate synchrotron microbeam radiation therapy. Preclinical evidence in view of a clinical transfer *Radiother. Oncol.* **139** 56–61
[12] Fernandez-Palomo C *et al* 2020 Complete remission of mouse melanoma after temporally fractionated microbeam radiotherapy *Cancers (Basel).* **12** 1–13
[13] Fernandez-Palomo C *et al* 2020 Animal models in microbeam radiation therapy: a scoping review *Cancers (Basel).* **12** 527
[14] Trappetti V *et al* 2021 Microbeam radiotherapy—a novel therapeutic approach to overcome radioresistance and enhance anti-tumour response in melanoma *Int. J. Mol. Sci.* **22** 7755
[15] Potez M *et al* 2019 Synchrotron microbeam radiation therapy as a new approach for the treatment of radioresistant melanoma: potential underlying mechanisms *Int. J. Radiat. Oncol. Biol. Phys.* **105** 1126–36

[16] Schneider T et al 2022 Combining FLASH and spatially fractionated radiation therapy: the best of both worlds Radiother. Oncol. 175 169–177
[17] Schültke E et al 2021 A mouse model for microbeam radiation therapy of the lung Int. J. Radiat. Oncol. Biol. Phys. 110 521
[18] Trappetti V et al 2021 Synchrotron microbeam radiation therapy for the treatment of lung carcinoma: a preclinical study Int. J. Radiat. Oncol. Biol. Phys. 111 1276–88
[19] Trappetti V et al 2022 Microbeam radiation therapy controls local growth of radioresistant melanoma and treats out-of-field locoregional metastasis Int. J. Radiat. Oncol. Biol. Phys. 114 478–493
[20] Fernandez-Palomo C, Chang S and Prezado Y 2022 Should Peak dose be used to prescribe spatially fractionated radiation therapy?—a review of preclinical studies Cancers (Basel). 14 7–14
[21] Fernandez-Palomo C et al 2022 Non-targeted effects of synchrotron radiation: lessons from experiments at the australian and european synchrotrons Applied Sciences (Switzerland). 12 1–20
[22] Duncan M, Donzelli M, Pellicioli P, Brauer-Krisch E, Davis J A, Michael L F L, Anatoly B, Rosenfeld and Petasecca M 2019 First experimental measurement of the effect of cardio-synchronous brain motion on the dose distribution during microbeam radiation therapy Med. Phys. 47 213–22
[23] Donzelli M, Bräuer-Krisch E and Oelfke U 2016 Brain motion induced artefacts in microbeam radiation therapy: a Monte Carlo study Radiother. Oncol. 118 ESTRO 35 2016
[24] Bartzsch S et al 2020 Technical advances in x-ray microbeam radiation therapy Phys. Med. Biol. 65 02TR01
[25] Livingstone J et al 2017 Preclinical radiotherapy at the australian synchrotron's imaging and medical beamline: instrumentation, dosimetry and a small-animal feasibility study J. Synchrotron Radiat. 24 854
[26] Stevenson A W et al 2010 First experiments on the australian synchrotron imaging and medical beamline, including investigations of the effective source size in respect of x-ray imaging J. Synchrotron Radiat. 17 75–80
[27] Wysokinski T W et al 2013 Beamlines of the biomedical imaging and therapy facility at the canadian light source - Part 2 J. Phys. Conf. Ser. 425 072013
[28] Wysokinski T W et al 2015 Beamlines of the biomedical imaging and therapy facility at the canadian light source—part 3 Nucl. Instrum. Methods Phys. Res. A 775 1–4
[29] Uyama A et al 2011 A narrow microbeam is more effective for tumor growth suppression than a wide microbeam: an in vivo study using implanted human glioma cells J. Synchrotron Radiat. 18 671–8
[30] Schültke E et al 2022 The microbeam insert at the white beam beamline P61A at the synchrotron PETRA III/DESY: a new tool for high dose rate irradiation research Cancers (Basel). 14 5137
[31] Siegbahn E A et al 2006 Determination of dosimetrical quantities used in microbeam radiation therapy (MRT) with Monte Carlo simulations Med. Phys. 33 3248–59
[32] Crosbie J C et al 2015 Energy spectra considerations for synchrotron radiotherapy trials on the ID17 bio-medical beamline at the european synchrotron radiation facility J. Synchrotron Radiat. 22 1035–41
[33] Rebuffi L and Sanchez del Rio M 2017 OASYS (OrAnge SYnchrotron Suite): an open-source graphical environment for x-ray virtual experiments Advances in Computational Methods for X-Ray Optics IV. ed K Sawhney and O Chubar (San Diego, California, United States: SPIE) 10388, 28
[34] Mayles P, Nahum A and Rosenwald J C 2007 Handbook of Radiotherapy Physics. (London: CRC Press) (https://doi.org/10.1201/9781420012026)
[35] Vatnitsky S M 2008 International atomic energy agency. commissioning of radiotherapy treatment planning systems: testing for typical external beam treatment techniques Commissioning of Radiotherapy Treatment Planning Systems: Testing for Typical External Beam Treatment Techniques. (Vienna, Austria: International Atomic Energy Agency) 1–76 Vienna, Austria978-92-0-100508-3
[36] Berkvens P et al 2013 Highly robust, high intensity white synchrotron beam monitor IEEE Nuclear Science Symp. Conf. Record. Institute of Electrical and Electronics Engineers Inc (https://doi.org/10.1109/NSSMIC.2013.6829691)
[37] Requardt H et al 2013 A new gas attenuator system for the ID17 biomedical beamline at the ESRF J. Phys. Conf. Ser. 425 022002
[38] Sánchez del Río M and Dejus R J 2011 XOP v2.4: recent developments of the x-ray optics software toolkit Advances in Computational Methods for X-Ray Optics II. ed M Sanchez del Rio and O Chubar (San Diego, California, United States: SPIE Optical Engineering + Applications) 8141814115 (https://doi.org/10.1117/12.893911)
[39] Raimondi P et al 2023 The Extremely brilliant source storage ring of the european synchrotron radiation facility Commun. Phys. 6 82
[40] Elam W T, Ravel B D and Sieber J 2002 A new atomic database for x-ray spectroscopic calculations Radiat. Phys. Chem. 63 121–8
[41] Fournier P et al 2016 Absorbed dose-to-water protocol applied to synchrotron-generated x-rays at very high dose rates Phys. Med. Biol. 61 N349–61
[42] Musolino S V and IAEA TRS-398 2001 Absorbed dose determination in external beam radiotherapy: an international code of practice for dosimetry based on standards of absorbed dose to water Technical Reports Series No. 398 81 592
[43] Butler D J et al 2016 Absorbed dose determination in kilovoltage x-ray synchrotron radiation using alanine dosimeters Australas. Phys. Eng. Sci. Med. 39 943–50
[44] Donzelli M et al 2018 Hybrid dose calculation: a dose calculation algorithm for microbeam radiation therapy Phys. Med. Biol. 63 045013
[45] Agostinelli S et al 2003 GEANT4 - a simulation toolkit Nucl. Instrum. Methods Phys. Res. A 506 250–303
[46] Salvat F, Fernández-Vera J and Sempau J 2009 PENELOPE-2008: a code system for monte carlo simulation of electron and photon transport Simulation 6 324
[47] Day L R J et al 2021 A commercial treatment planning system with a hybrid dose calculation algorithm for synchrotron radiotherapy trials Phys. Med. Biol. 66 055016
[48] Poole C M et al 2017 Synchrotron microbeam radiotherapy in a commercially available treatment planning system Biomed. Phys. Eng. Express 3 025001
[49] Williams M and Metcalfe P 2011 Radiochromic film dosimetry and its applications in radiotherapy AIP Conf. Proc. 1345 75–99
[50] Pellicioli P et al 2019 High resolution radiochromic film dosimetry: comparison of a microdensitometer and an optical microscope Physica Med. 65 106–13
[51] Downey A S, Delaney L J and Morrow J B 2014 10.6028/NIST.NSRDS.164
[52] Pellicioli P et al 2021 Study of the x-ray radiation interaction with a multislit collimator for the creation of microbeams in radiation therapy J. Synchrotron Radiat. 28 392–403